ACS OMEGA

http://pubs.acs.org/journal/acsodf

Article

Nanoindentation for Monitoring the Time-Variant Mechanical Strength of Drug-Loaded Collagen Hydrogel Regulated by Hydroxyapatite Nanoparticles

Hyo Gi Jung,[#] Dongtak Lee,[#] Sang Won Lee, Insu Kim, Yonghwan Kim, Jae Won Jang, Jeong Hoon Lee, Gyudo Lee,[*] and Dae Sung Yoon[*]

Cite This: *ACS Omega* 2021, 6, 9269−9278

Read Online

ACCESS | Metrics & More | Article Recommendations | Supporting Information

ABSTRACT: Hydroxyapatite nanoparticle-complexed collagen (HAP/Col) hydrogels have been widely used in biomedical applications as a scaffold for controlled drug release (DR). The time-variant mechanical properties (Young's modulus, E) of HAP/Col hydrogels are highly relevant to the precise and efficient control of DR. However, the correlation between the DR and the E of hydrogels remains unclear because of the lack of a nondestructive and continuous measuring system. To reveal the correlations, herein, we investigate the time-variant behavior of E for HAP/Col hydrogels during 28 days using the atomic force microscopy (AFM) nanoindentation technique. The initial E of hydrogels was controlled from 200 to 9000 Pa by the addition of HAPs. Subsequently, we analyzed the relationship between the DR of the hydrogels and the changes in their mechanical properties (ΔE) during hydrogel degradation. Interestingly, the higher the initial E value of HAP/Col hydrogels is, the higher is the rate of hydrogel degradation over time. However, the DR of hydrogels with higher initial E appeared to be significantly delayed by up to 40% at a maximum. The results indicate that adding an appropriate amount of HAPs into hydrogels plays a crucial role in determining the initial E and their degradation rate, which can contribute to the properties that prolong DR. Our findings may provide insights into designing hydrogels for biomedical applications such as bone regeneration and drug-delivery systems.

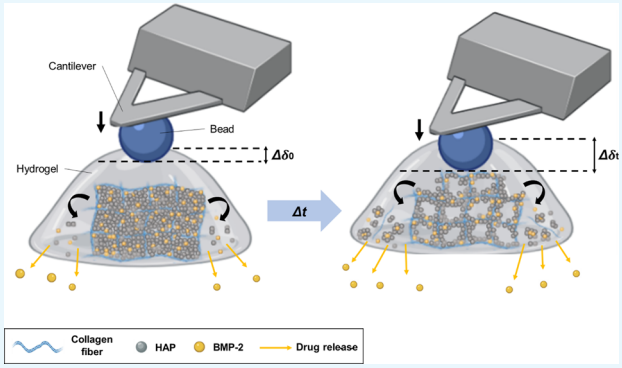

1. INTRODUCTION

Hydrogels are a well-known material with a polymeric network in which the polymer chains are very hydrophilic, making them capable of associating with large quantities of water or biological fluids without dissolving.[1−3] Because of a large proportion of water in the human body, hydrogels have a great potential for drug delivery.[2,4,5] This is because they can protect the drug from environmental challenges and control drug release (DR) by maintaining their structure.[1,6] Biodegradable hydrogels also present considerable advantages in drug delivery, including excellent biocompatibility, flexibility in controlling complex stability, and easy control of drug diffusion kinetics.[7] Hydrogels with these advantages can be used in diverse delivery systems designed for transporting various compounds such as drugs, small molecules, DNA, proteins, and even cells.[6,8] In particular, the hydrogels containing Food and Drug Administration (FDA)-approved proteins (e.g., bone morphogenic protein-2 and BMP-2) have been used for therapeutic purposes (e.g., bone regeneration) by enhancing the protein's pharmacokinetic and pharmacodynamic properties.[9−15]

Controlling the mechanical properties of a hydrogel is an essential strategy for improving the ability to modulate DR. Researchers have used several methods including physical and chemical cross-linking methods[16] to control the mechanical properties of hydrogels and studied how effective they are for the DR kinetics. The adoption of ultraviolet (UV) irradiation with mediators is the most common cross-linking method for various hydrogels because of the advantages of safety, cost effectiveness, and shorter durations of time for gel formation. Various studies using UV cross-linking have shown that the drug release rate from the hydrogel can be delayed by modulating the mechanical properties of hydrogels.[17,18] There are also previous studies that show the relationship between the mechanical properties and the DR by hydrogels using

Received: February 15, 2021
Accepted: March 2, 2021
Published: March 23, 2021

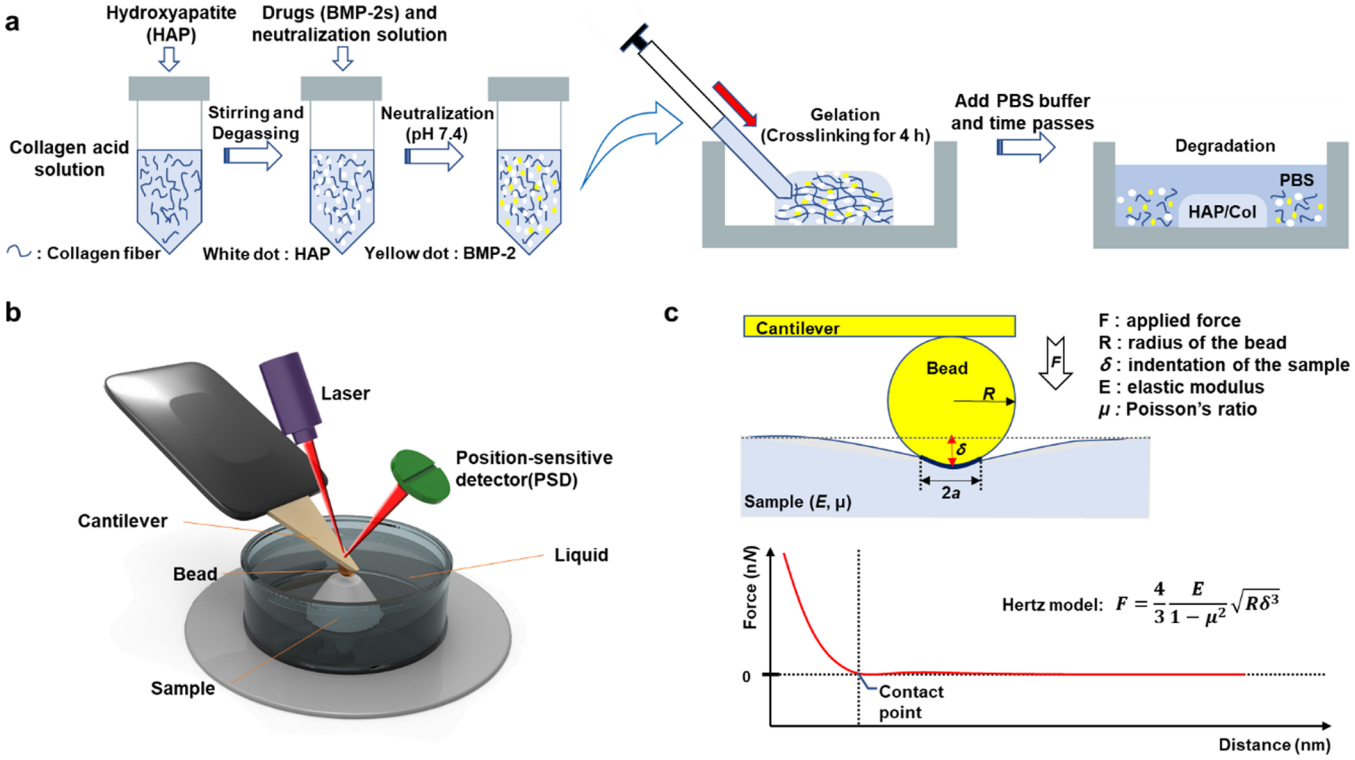

Figure 1. Schematic illustration of the AFM nanoindentation strategy for measuring the Young's modulus (E) of the HAP/Col hydrogels. (a) Fabrication process of the collagen fibers (blue thread) which were mixed with the HAPs (white dot) by stirring at 10,000 rpm. The BMP-2 and neutralization solution were added to the collagen slurry, and the cross-linking process was conducted at 37 °C for 4 h. After that, the HAP/Col hydrogel was incubated in the PBS solution at 37 °C to mimic physiological conditions. (b) Schematic illustration of AFM nanoindentation in the aqueous solution. Pressing the sample with the bead causes the cantilever to deflect and change the degree of reflection of the laser. The detector senses the change in the laser value, which allows the measurement of the surface modulus of the sample. (c) Hertz model for analyzing the E value of the HAP/Col hydrogel. This model is based on the contact between a sphere and a half space, showing the F−D curve-based AFM, which contours the surface of the sample while recording a pixel-by-pixel full F−D curve.

various mediators.[19−21] Martinez et al. used cross-linking via many other methods including genipin, glutaraldehyde (GTA), GTA vapor cross-linking, disulfide (SS), and SS vapor cross-linking.[21] They revealed that DR is inversely related to the degree of cross-linking or physical chain entanglements that were related to the mechanical properties of the hydrogel. The findings imply that regulating the mechanical properties of the hydrogel is critical for the fine control of its DR rate.

However, the pure hydrogels are peculiar materials that have relatively small elastic modulus values and exhibit neither the behavior of solids nor liquids. The design and function of pharmaceutical hydrogels may be limited by their relatively low stiffness and strength because of their porous structure and the substantial fraction of water they contain.[22] Accordingly, researchers have faced significant challenges in measuring the mechanical properties of the hydrogels and interpreting their mechanical data. A primary hurdle is the measurement of the mechanical properties of the sample (in particular, Young's modulus, E) using nondestructive methods.[23] It is because most hydrogels have the order of kiloPascals (kPa) of E, while most mechanical testing equipment is optimized for testing in the range from megapascals (MPa) to gigapascals (GPa).[24] Furthermore, the hydrogels exhibit various local stiffness location-by-location because they consist of a porous network with a liquid phase.[24] For this reason, the relationship between the E and the DR of hydrogels remains poorly defined.[4]

To reveal the correlation between the E and DR of the hydrogels, we prepared collagen hydrogels containing bone morphogenic protein-2 (BMP-2) as a model protein drug. The E of hydrogels was controlled by the addition of hydroxyapatite nanoparticles (HAPs). We used atomic force microscopy (AFM), which is the most versatile and powerful microscopic technology for analyzing samples at the nanoscale.[25−27] Among the various applications of AFM, we operated the nanoindentation test using an AFM cantilever with a 10.8 μm bead (Figure 1). We provided a quantitative analysis of the time-variant nanomechanical behavior of the hydrogels with different HAP concentrations. We also investigated the DR of each hydrogel using the enzyme-linked immunosorbent assay (ELISA). The results demonstrated that the initial nanomechanical properties of the hydrogel play a pivotal role in controlling its DR. We believed that our approach can help researchers to properly design hydrogels for biomedical applications such as bone-regenerative medicines and drug-delivery system.

2. EXPERIMENTAL SECTION

2.1. Materials. To fabricate three-dimensional (3D)-structured hydrogels, we prepared both rat tail-derived collagen type I solution (3.8 mg/mL) and neutralization solution from Advanced BioMatrix (USA). We purchased a recombinant human bone morphogenic protein-2 (rhBMP-2) from Peprotech (USA) and the HAP nanoparticles (<200 nm) from Sigma Aldrich (USA) (Figure S1, Supporting Information). The ELISA kits (Koma Biotech, South Korea) were used for the rhBMP-2 assay.

https://doi.org/10.1021/acsomega.1c00824
ACS Omega 2021, 6, 9269−9278

2.2. HAP/Col Hydrogel Fabrication. We fabricated four types of collagen hydrogels with different mass ratios of HAP and collagen type I: HAP/Col (0/3.8), HAP/Col (100/3.8), HAP/Col (200/3.8), and HAP/Col (400/3.8). To prevent an unintended gelation of collagen, all the fabrication steps were performed at less than 4 °C. We added 2 mL of collagen solution (3.8 mg/mL) to each vial and stirred it with 0 (negative control), 200, 400, and 800 mg of HAPs. To obtain a uniformly stirred solution, each solution was blended at 10,000 rpm for 10 min using a homogenizer (Daihan Scientific, South Korea). The blended solutions were degassed under vacuum to remove air bubbles before fabricating the homogeneous HAP/Col hydrogels. After degassing, the HAP/Col solution was gently mixed with 2 μg of BMP-2, and 0.2 mL of neutralization solution was added to induce the sol-to-gel transition of the HAP/Col solution. Then, the HAP/Col solution (1 mL) was placed into a petri dish and incubated at 37 °C for 4 h until gelation of the HAP/Col hydrogel.

2.3. Characterization of the HAP/Col Hydrogels. The HAP/Col hydrogels were lyophilized at 5 mTorr and 80 °C for 12 h using a freezer dryer (ilShinbiobase, South Korea) to analyze their characteristics. The dried HAP/Col hydrogels were soaked in distilled water to hydrate and were taken out to measure the swelling performance. The maximum swelling ratio was obtained using the following eq 1, where W_d is a weight of the dried hydrogel, and W_s is the maximum weight of the swelled hydrogel.

$$\text{Maximum swelling ratio} \equiv \frac{W_s - W_d}{W_d} \times 100\ (\%) \tag{1}$$

The morphological property of the lyophilized HAP/Col composites was characterized by scanning electron microscopy (SEM) (JSM-6701F, JEOL, Japan). For the SEM imaging, the HAP/Col hydrogels (8 mm in diameter and 2 mm in height) were placed onto metallic stubs on carbon tape and sputtered with gold (Au) plasma for 120 s. The SEM images were obtained at 5 kV using the secondary electron mode taken at a working distance between 8 and 10 mm. The Fourier-transform infrared (FTIR) spectra were analyzed using a Vertex 70 instrument (Bruker, USA). Each spectrum was collected in the range of 400 to 4000 cm^{-1}, and it was acquired via an accumulation of 256 scans with a resolution of 4 cm^{-1}. X-ray diffraction (XRD) patterns were obtained using an Ultima IV instrument (Rigaku, USA) operating with a Cu anticathode. A diffraction range of 10−70° (2θ) was selected, and the XRD analysis was carried out at 2°/min. Thermogravimetric analysis (TGA) was carried out using a Q50 (TA Instrument, USA). In detail, the samples were heated from room temperature to 500 °C at a heating rate of 20 °C/min under a nitrogen flow. The rheological measurements of the HAP/Col hydrogels were performed using a rheometer (HAKKE MARS, Thermo Fisher Scientific, USA) at 20 °C with a parallel plate geometry. The strains were chosen to be in the linear viscoelastic range, where the storage modulus (G') and the loss modulus (G'') were independent of the oscillation stress. After a strain sweep test, the frequency sweeps were conducted in the linear viscoelastic ranges which were 0.056 to 1.006 Pa, 0.361 to 1.001 Pa, 0.382 to 1.002 Pa, and 1.000 to 1.994 Pa for the HAP/Col hydrogels (0/3.8, 100/3.8, 200/3.8, and 400/3.8), respectively.

2.4. In Vitro Drug Release Test. To examine the BMP-2 release profile of the HAP/Col hydrogels, the hydrogels were deposited in 3 mL of the phosphate-buffered saline (PBS) solution and placed in a shaking incubator (WIS-20, Daihan scientific, South Korea) which was maintained at 37 °C. We replaced the release media samples (i.e., PBS solution) to the fresh PBS solution at the given time points during 28 days. The concentration of the drug released from the hydrogels was measured using a microplate reader (Versa Max, Molecular Devices, USA) using a rhBMP-2 ELISA kit (KOMA biotech, South Korea). To normalize the DR of each HAP/Col hydrogel, we defined the relative DR as the following eq 2:

$$\text{Relative DR} \equiv \frac{\text{Cumulative DR at each time point}}{\text{DR at 1 day}} \times 100\ (\%) \tag{2}$$

2.5. AFM Nanoindentation of the HAP/Col Hydrogel. The Young's modulus (E, Pa) of each HAP/Col hydrogel was measured using an atomic force microscope (Park NX10 AFM, Park System, South Korea) in a liquid phase (i.e., PBS solution). Using this process, we measured the nano-mechanical properties of the hydrogel with nondestructive nanoindentation. We used a silicon nitride AFM cantilever (CP-PNP-PS, NanoAndMore, USA) that has a nominal spring constant (~0.08 N/m) and has a 10.8 μm polystyrene bead attached to the end of the cantilever.[28] The E (i.e., mechanical strength) was calculated using the Hertz model, as follows (eq 3. Here, F indicates the applied force, R is the radius of the sphere, δ is an indentation depth, and μ is the Poisson ratio (0.5) of hydrogels that are assumed to be a linearly elastic isotropic network.[29]

$$F = \frac{4}{3}\frac{E}{1-\mu^2}\sqrt{R\delta^3} \tag{3}$$

We calibrated both the axis (x-axis and y-axis) of the AFM sample stage using a Smart Scan software (Park Systems, South Korea) before measuring the E of the HAP/Col hydrogel. Also, the nanoindentation measuring system was calibrated at room temperature to measure the spring constant of the cantilever through the thermal noise method.[30] During all the experiments, the approach and retraction velocities of the AFM cantilever were maintained at 1 μm/s, and the cantilever was ramped by 4 μm with a 5 nN threshold in a closed z-loop. A force−distance (F−D) curve was fitted using XEI software (Park Systems, South Korea). We fitted the curves using the Hertz model from the contact point to the endpoint of the curve for eliminating the errors originating from the ill-defined contact points.[31]

3. RESULTS AND DISCUSSION

3.1. AFM Nanoindentation Strategy for Measuring the Mechanical Strength (E) of the HAP/Col Hydrogels. We fabricated four different types of HAP/Col hydrogels with different HAP concentrations. Under low pH and low-temperature conditions, soluble collagen monomers do not undergo further chemical cross-linking.[32] On the other hand, by adding to a neutral solution at 37 °C, the conversion of Lys/Hyl residues located in the nonhelical C- and N-telopeptides of collagen molecules causes the covalent intermolecular cross-linking of collagens.[33] After cross-linking the HAP/Col hydrogels on a petri dish, we added the PBS (pH 7.4) to analyze the DR at 37 °C, under mimic physiological conditions (Figure 1a). Because the HAP/Col hydrogels were hydrated and degraded with time, the drug was released into

https://doi.org/10.1021/acsomega.1c00824
ACS Omega 2021, 6, 9269−9278

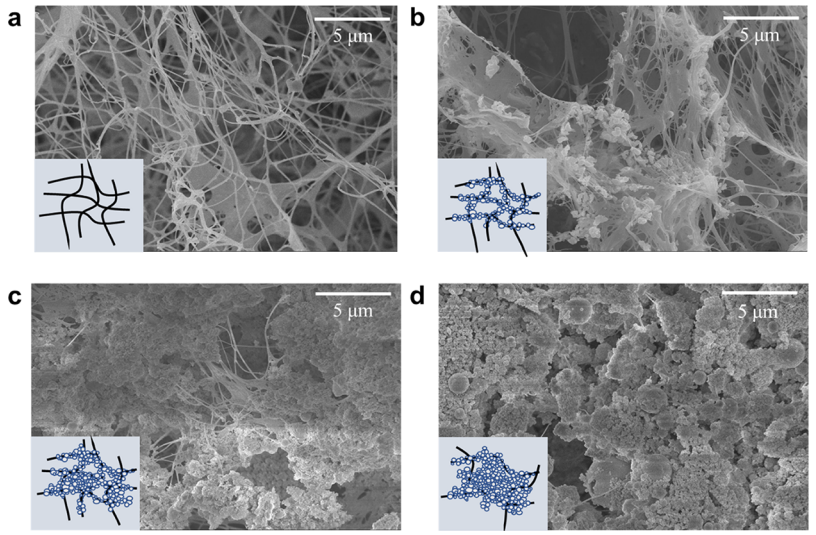

Figure 2. SEM images of the HAP/Col hydrogels depending on the HAP concentration. (a) HAP/Col (0/3.8) hydrogel, (b) HAP/Col (100/3.8) hydrogel, (c) HAP/Col (200/3.8) hydrogel, and (d) HAP/Col (400/3.8) hydrogel. The schematic illustration inserted in the SEM image showed the approximate conformational structure of each HAP/Col hydrogel composed of collagen fibers (black) and HAPs (white).

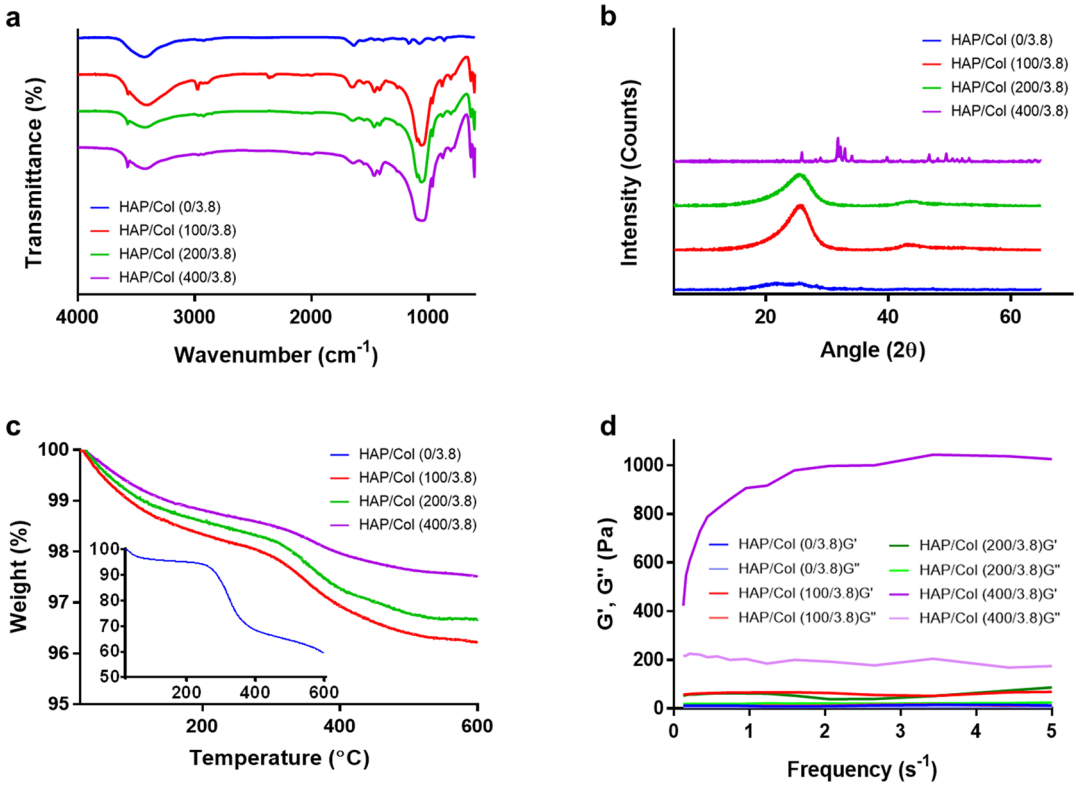

Figure 3. Physicochemical properties of the HAP/Col hydrogels. a) FTIR spectra, b) XRD patterns, c) TGA, and d) rheological test of the HAP/Col hydrogels with different HAP concentrations (i.e., HAP/Col hydrogels (0/3.8, 100/3.8, 200/3.8, and 400/3.8)).

the buffer. At given time points up to 28 days, the release media was sampled and replaced with fresh PBS solution each time. For nondestructive AFM nanoindentation, we used a 10.8 μm polystyrene bead-functionalized AFM cantilever with a spring constant of 0.08 N/m (Figure 1b). As the AFM cantilever was loaded to the gel surface, we could measure the F−D curves of each HAP/Col hydrogel in the PBS solution (Figure 1c). Once an AFM cantilever is indented into the HAP/Col hydrogel, the mechanical contact between the bead and the gel surface causes a deflection of the cantilever. The deformation of the cantilever created a change in the laser displacement on the position-sensitive detector (PSD), and the result was recorded as the F−D curves. Upon analyzing the F−D curves, we adopted the Hertz model to determine E of the hydrogel (Figure 1c). The model is related to the applied loading force F and the indentation depth or deformation δ (see Experimental method 2.5). We could obtain detailed information about the E of different hydrogel formulations by analyzing the F−D curves, indicating the applied force versus displacement behavior of hydrogels.

https://doi.org/10.1021/acsomega.1c00824
ACS Omega 2021, 6, 9269−9278

3.2. Morphological Properties of the HAP/Col Hydrogels. We performed SEM imaging to observe the morphological characterization of the HAP/Col hydrogels (Figure 2). The morphological properties of the HAP/Col hydrogels were significantly different depending on the HAP concentration. Specifically, the HAP/Col (0/3.8) hydrogel consists of a porous structure with only collagen fibers (Figure 2a). In the case of the HAP/Col (100/3.8) hydrogel, the porous structure was maintained with HAPs attached to the collagen fibers (Figure 2b). It is attributed to the strong affinity between the collagen fiber and HAPs.[34] On the other hand, the porosity of the HAP/Col (200/3.8) hydrogel was significantly reduced because the HAPs aggregated each other and efficiently occupied empty spaces inside the hydrogel (Figure 2c). This arrangement is thought to make the hydrogel stiffer. At the highest HAP concentration (HAP/Col (400/3.8) hydrogel), its porous structure almost disappeared, and the gel surface was covered with massive HAPs (Figure 2d). The large HAP aggregates filled the pore structure between the collagen fibers, which decreased the porosity. We measured the nanomechanical strength of the HAP/Col hydrogels using the 10.8 μm polystyrene-bead tip. Because the size of the AFM probe tip is much larger than the pore of each hydrogel, it is assumed that the diverse pore size of the hydrogel hardly influenced the estimation of the nanomechanical properties of the HAP/Col hydrogels.[35]

3.3. Physicochemical Properties of the HAP/Col Hydrogels. To investigate the physicochemical properties of the HAP/Col hydrogels, we conducted several experiments including the swelling test, Fourier-transform infrared spectroscopy (FTIR), X-ray diffraction (XRD), thermogravimetric analysis (TGA), and rheometry. As shown in Table S1, the maximum swelling ratio of each hydrogel decreased in a manner dependent on the HAP concentration because the pore structures between the collagen fibers are filled with HAPs instead of water molecules. Figure 3a and Figure S2a showed the FTIR spectra of the HAP/Col hydrogels including IR absorbance peaks corresponding to collagen and HAPs. In detail, the HAP/Col (0/3.8) hydrogel indicated intrinsic peaks at 1633, 1556, and 3000−3600 cm^{-1} corresponding to the amide I, amide II, and OH group.[36] The HAP/Col hydrogels (100/3.8, 200/3.8, and 400/3.8) depicted not only the peaks of the pure collagen but also the peaks of the combination of HAPs and collagen at 1400−1480 cm^{-1} from CO_3^{2-} absorption.[37] It indicated the HAPs in the hydrogels being partially carbonated.[38] The absorption bands of the phosphate stretching vibration were also identified at 950−1050 cm^{-1}, which is due to the HAPs containing multiple phosphate ions.[39] The XRD analysis was performed to identify the crystalline species of hydrogels with different HAP proportions (Figure 3b and Figure S2b, Supporting Information). The HAP/Col (0/3.8) hydrogel exhibited a broad peak at 10−25° in 2θ, which is typical for collagen fibers.[40] In contrast, the diffraction pattern of hydrogels (100/3.8 and 200/3.8) showed a broad peak at around 26° in 2θ, which corresponds to the (002) HAP.[40] The HAP/Col (400/3.8) hydrogel exhibited very sharp peaks, which were identical to the powder diffraction pattern of the HAP.[40] For instance, the peaks of the HAP/Col (400/3.8) hydrogel at around 26° and 32° corresponded to the (002) and (211) HAP.[40] These results indicated that the surface of the HAP/Col hydrogel at a ratio of 400/3.8 was massively covered with HAPs, hiding the collagen networks.[41]

To understand the thermal behavior of hydrogels, we performed TGA (Figure 3c). The results showed that as the concentration of HAPs increased, the weight loss of hydrogels diminished. Gradual weight loss from the HAP/Col (0/3.8) hydrogel over the whole temperature range is known to occur because of several factors. From room temperature to 120 °C, the weight loss in the 0/3.8 hydrogel is due to the evaporation of adsorbed water.[42] In contrast, the weight loss at 220−440 °C is associated with the decomposition of the collagen molecules, and the slight weight loss seen at over 440 °C is owing to the combustion of the residual organic components.[42] Overall, the HAP/Col (0/3.8) hydrogel exhibits much more weight loss (∼40%) than that of others (2−4%) because it consists of pure collagen networks. For the HAP/Col hydrogels (100/3.8, 200/3.8, and 400/3.8), the weight loss at room temperature observed up to 250 °C is due to the depletion of water freely bound to the collagen and HAP, and the weight loss at 250−600 °C is attributed to the decomposition of the collagen molecules and the gradual dihydroxylation of HAP.[43] Derivative thermogravimetric (DTG) curves showed that two peaks appeared regardless of HAP concentration (Figure S3, Supporting Information). The peak values of the HAP/Col (0/3.8) hydrogel were over ten times larger than those of the HAP/Col hydrogels (100/3.8 and 200/3.8). In the case of HAP/Col (400/3.8) hydrogel, however, the peak value was dramatically lesser than even that of the HAP/Col hydrogels (100/3.8 and 200/3.8).[43] Accordingly, we can infer that the amount of collagen networks in the HAP/Col (400/3.8) hydrogel was lesser than that in others.

Rheological tests were performed to investigate the flow behavior of the HAP/Col hydrogels by oscillation stress sweep and frequency sweep. The results of the oscillation stress sweep showed that the G' and G'' of each HAP/Col hydrogel were independent of the oscillation stress sweep before deformation where the G'' rapidly decreases (Figure S4, Supporting Information).[44] As more HAPs were added, the G' and G'' before deformation gradually increased, indicating that the addition of HAPs significantly affected viscosity.[45] Dynamic frequency sweep tests showed the behavior of the G' and G'' of the hydrogels in the linear viscoelastic region as a function of angular frequency (Figure 3d). For each HAP/Col hydrogel, the G' was higher than the G'', indicative of the structural characteristics of hydrogels and occurs because their structure was reinforced by the cross-linking between the collagen fibers and the interactions between the collagen fibers and HAPs.[46] The G's of the HAP/Col hydrogels (0/3.8, 100/3.8, and 200/3.8) exhibited no significant change throughout the whole frequency range. For the HAP/Col (400/3.8) hydrogel, however, the G' was much higher, exhibiting significant changes depending on the frequency. Consequently, we can infer that the HAP/Col (400/3.8) hydrogel is stiff but retains more fluid-like properties, like cement slurry. These data demonstrated that the HAP/Col hydrogels lose their hydrogel-like nature by adding significant proportions of HAPs (>400 mg/mL).

3.4. Drug Release Profiles of the HAP/Col Hydrogels. To verify the performance of hydrogels for DR, the BMP-2 was loaded in all, and the DR profiles were then monitored for 28 days. Figure 4 shows the relative drug (i.e., BMP-2) release profile of the different HAP/Col hydrogels over time. The BMP-2 at different incubation times was measured to elucidate the relationship between the HAP concentration and DR

https://doi.org/10.1021/acsomega.1c00824
ACS Omega 2021, 6, 9269−9278

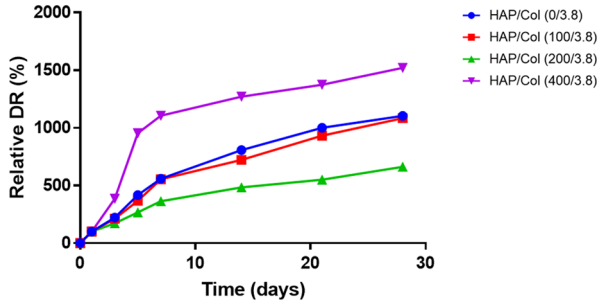

Figure 4. Relative BMP-2 release profile for four different conditions of HAP/Col hydrogels depending on the HAP concentration.

(Figure S5, Supporting Information). For the HAP/Col hydrogels (0/3.8, 100/3.8, and 200/3.8), the DR was gradually delayed as the HAP concentration increased. By 28 days, the relative amount of DR by HAP/Col hydrogels (100/3.8 and 200/3.8) was 1.8 and 40.0% less than that of pure collagen hydrogel. In the case of the HAP/Col (400/3.8) hydrogel, however, the BMP-2 was released rapidly at the beginning because it lost its nature of hydrogel and was easily fractured. These results imply that the HAP concentration is critical for maintaining both the property of the hydrogel as well as for controlling the rate of DR.

3.5. AFM Nanoindentation of the HAP/Col Hydrogels.

Using the AFM nanoindentation technique, we acquired the F−D curves for the HAP/Col hydrogels of different compositions (Figure S6, Supporting Information). The slopes of the F−D curves for each HAP/Col hydrogel became steeper with increase in the HAP concentration, indicating that E increased. Next, we performed the time-variant nanomechanical tests of each hydrogel for 28 days (Figure 5). The detailed E distribution of each hydrogel over time is described in Figure 5a−e. For each hydrogel, the more HAPs it contains, the higher the average E and the wider the E distribution observed. Therefore, as the HAP concentration increases, the hydrogel becomes stiff and nonuniform, implying that the HAPs heterogeneously fill the porous structure of the hydrogel.[47] As time passes, the E distributions of all the HAP/Col hydrogels are skewed to the left and become narrower. Specifically, Figure 5f shows the changes in the E of each HAP/Col hydrogel over time. The average Es of the fresh hydrogels were estimated to be 323 ± 38, 747 ± 369, 2635 ± 924, and 8656 ± 4166 Pa for the HAP/Col hydrogels (0/3.8, 100/3.8, 200/3.8, and 400/3.8), respectively. After 28 days, the Es were estimated to be 199 ± 27, 388 ± 33, 780 ± 199, and 1159 ± 227 Pa for HAP/Col hydrogels (0/3.8, 100/3.8, 200/3.8, and 400/3.8), respectively. The decrease in E over time is due to the gradual degradation of the hydrogel caused by the hydration and subsequent decomposition of collagen fibers and HAPs.[48] It is observed that the HAP/Col hydrogel with a high concentration of HAP tends to have a dramatic change of E with degradation.

The time-variant nanomechanical properties of each hydrogel were analyzed by linear fitting (1−21 days) (Figure S7, Supporting Information). Specifically, the $\Delta E/\Delta t$ (i.e., the absolute value of the slope of each linear regression curve) of the HAP/Col hydrogels (0/3.8, 100/3.8, 200/3.8, and 400/3.8) were 6.71 ± 0.99, 14.11 ± 2.78, 83.24 ± 12.47, and 362.9 ± 46.9 Pa/day, respectively. These results indicated that the rate of hydrogel decomposition (i.e., $\Delta E/\Delta t$) was proportional to the initial E (R^2 = 0.998). When the HAP/Col hydrogels were fabricated with high concentrations of HAP, they

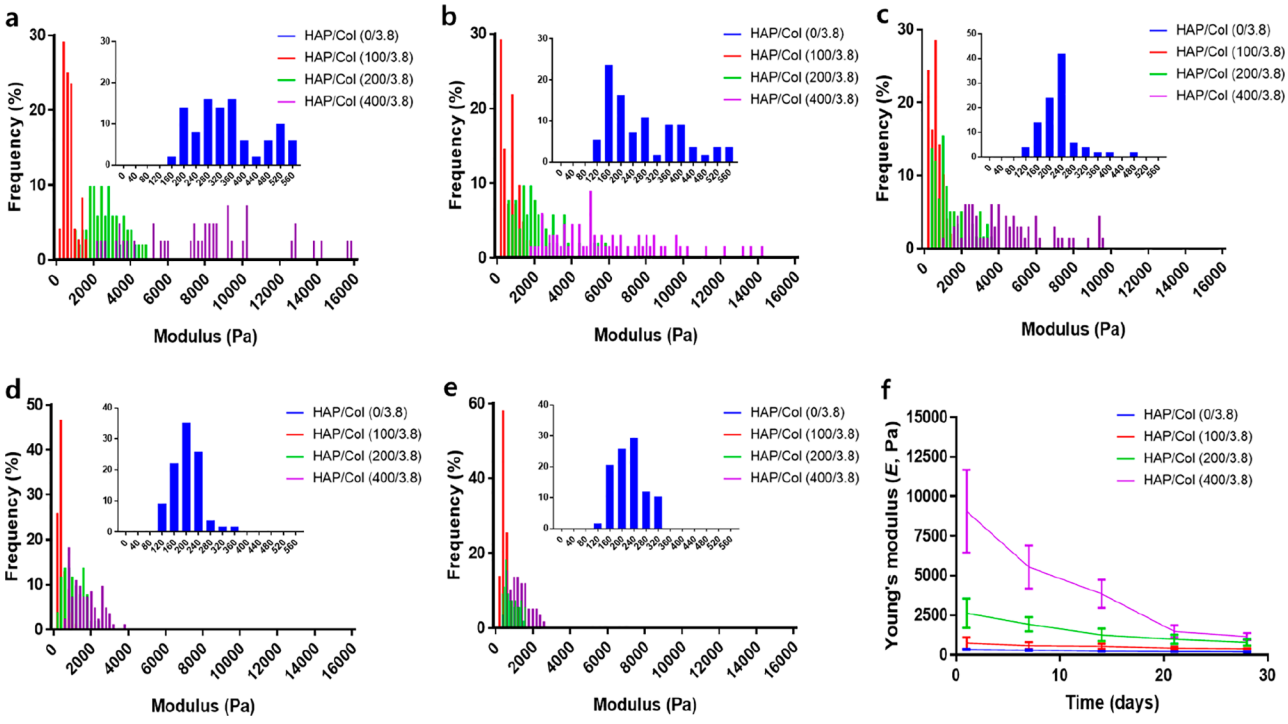

Figure 5. Time-variant AFM nanoindentation of the HAP/Col hydrogels. Histograms of the E for the HAP/Col (0/0.8, 100/3.8, 200/3.8, and 400/3.8) hydrogels with time: (a) 1 day, (b) 7 days, (c) 14 days, (d) 21 days, and (e) 28 days. The inserted data is the HAP/Col hydrogel (0/3.8) and the distribution of E for HAP/Col hydrogels narrows over time from 1 day to 28 days. (f) Time-variant E values of the HAP/Col hydrogels. For a HAP/Col (0/3.8) hydrogel, the detailed experimental results are provided in Figure S6 (see Supporting Information).

https://doi.org/10.1021/acsomega.1c00824
ACS Omega 2021, 6, 9269−9278

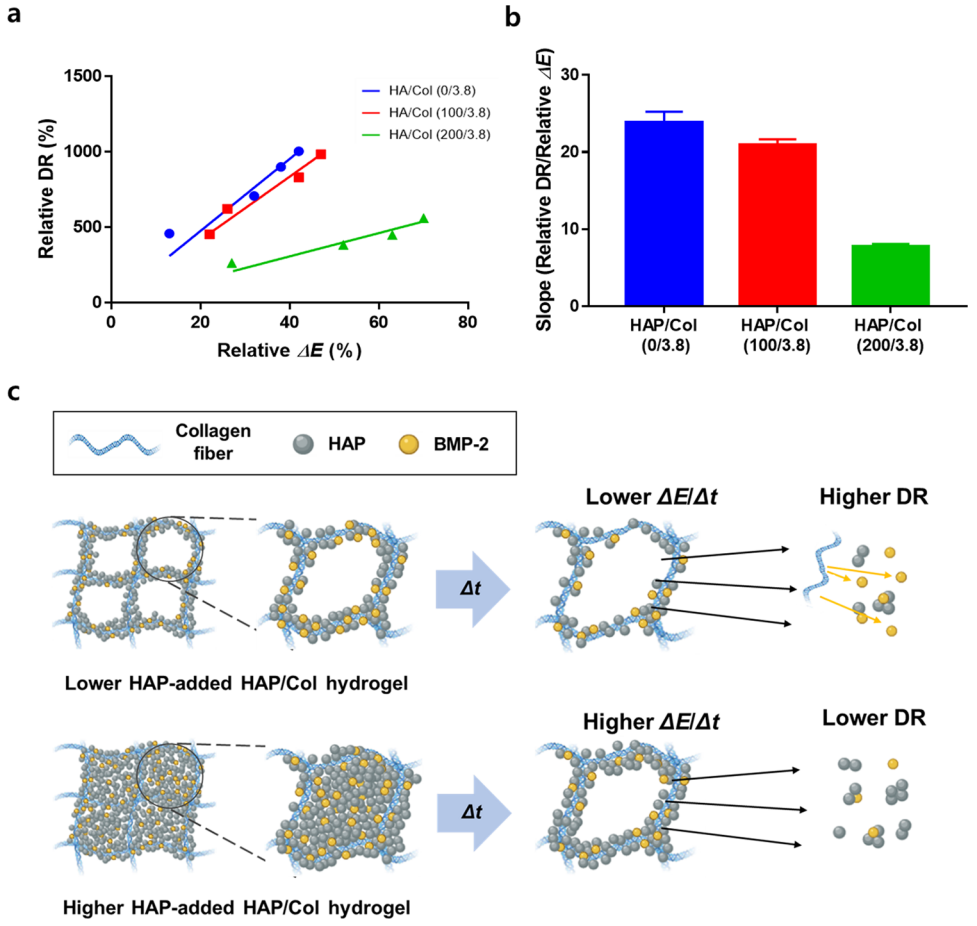

Figure 6. Relationship between time-dependent change in the Young's modulus (ΔE) of the HAP/Col hydrogels and the relative DR. (a) Dot plots of each HAP/Col hydrogel for analyzing the correlation between ΔE and relative DR. The plots were fitted by linear regression. (b) Value of the line slope of each HAP/Col hydrogel. The slope values of the 0/3.8, 100/3.8, and 200/3.8 hydrogels were calculated to be 23.86 ± 1.38, 20.92 ± 0.74, and 7.71 ± 0.37, respectively. (c) Schematic illustrated the degradation mechanisms of the HAP/Col hydrogels as the HAP concentration increases.

possessed excessive HAPs that were not bound to the collagen fiber. Accordingly, these nonbound HAPs were readily liberated from the hydrogel under aqueous conditions, inducing the large decrease in E observed with decomposition.[49]

3.6. Correlation between the Drug Release and Mechanical Strength of the HAP/Col Hydrogels. We investigated the correlation between the relative ΔEs and their DR kinetics using the HAP/Col hydrogels (0/3.8, 100/3.8, and 200/3.8) (Figure 6a). Herein, we defined the relative ΔE as the following eq 4:

$$\text{Relative } \Delta E \equiv \frac{\text{Cumulative } \Delta E \text{ at each time point}}{\text{Initial } E \text{ for each hydrogel}} \times 100 \ (\%) \quad (4)$$

We excluded the data for the HAP/Col (400/3.8) hydrogel because its properties are far from the usual nature of the hydrogel. This analysis showed that the relative DR of each hydrogel increased as a function of relative ΔE. This occurred because the decomposition-related decrease in E subsequently triggers the release of drugs.[6] The correlations between the relative DR versus the relative ΔE by linear regression were 23.86 ± 1.38, 20.92 ± 0.74, and 7.71 ± 0.37 for the HAP/Col hydrogels (0/3.8, 100/3.8, and 200/3.8), respectively (Figure 6b). The correlation values of the HAP/Col hydrogels (100/3.8 and 200/3.8) were decreased by 12.3 and 67.8% compared to the HAP/Col (0/3.8) hydrogel. Interestingly, the experimental results implied that the relative ΔE of each hydrogel increased as the HAP component increased, but its DR was delayed. The result can be explained by the following scenario (Figure 6c). In hydrogels without HAPs, the drugs (i.e., BMP-2) attached to the collagen fibers[50] and diffused into the PBS solution because of the direct hydration and subsequent degradation of collagen fibers. In contrast, for hydrogels with HAPs, the BMP-2 could bind to both the collagen fibers[50] and HAPs.[48] During the degradation process, the HAPs could physically block the interactions between the collagen fibers and water molecules by covering the surface of the collagen fibers containing BMP-2. As degradation continues, both HAPs and BMP-2 might become detached and diffuse into the PBS solution. In this respect, for the HAP/Col hydrogel (100/3.8), the extra HAPs did not fully cover the collagen surface, allowing direct contact between the solvent and fibers. This direct contact leads to complete degradation of hydrogel and its BMP-2 release.[51] On the other hand, the BMP-2 release rate was relatively slow in the case of HAP/Col hydrogel (200/3.8). This is because the degree of hydration and the subsequent degradation of collagen fiber are retarded by HAPs, delaying degradation and slowing the DR

https://doi.org/10.1021/acsomega.1c00824
ACS Omega 2021, 6, 9269−9278

kinetics.[52,53] It is to be noted that a steep change of relative ΔE occurred for the HAP/Col hydrogel (200/3.8) because the HAP detachment from the hydrogel induces its porous structure, which changes the indentation behavior.[54,55] In contrast, in the case of the HAP/Col hydrogel (100/3.8), the porous structure of the hydrogel was less affected by HAP detachment compared to that of the HAP/Col hydrogel (200/3.8), as shown in Figure 6c. These results indicated that adding an appropriate amount of HAPs into hydrogels plays a crucial role in determining their degradation rate and DR profiles. By analyzing the relative ΔE of the hydrogel and its relative DR, we extracted the correlation value between them and suggested a mechanism for controlling DR with additives (i.e., HAPs). We believe that this modeling and the correlation value could become one of the standard benchmarks to describe the characteristics of hydrogel-based DR, and this concept could be used to compare many other types of hydrogel systems in terms of DR.

4. CONCLUSIONS

We investigated time-dependent correlations between the nanomechanical properties of hydrogels and their DR using the AFM nanoindentation technique. We added the HAPs into the collagen hydrogels to control their initial E. As the amount of HAP increased, the initial E increased by 50 times in comparison with a hydrogel containing no HAPs. It was found that the change in the E of hydrogels strongly affected their DR. However, during the degradation of hydrogels under physiological conditions, our results showed that DR (i.e., BMP-2) is inversely proportional to the change in E. Specifically, the results indicated that the higher the initial E, the greater the sustainability of DR is, with the addition of HAPs into the hydrogels prolonging DR by ∼40%, compared to the hydrogels with no HAPs. In this regard, our concept of reinforcing the hydrogel with nanoparticles seems to be suitable for applications necessitating a low release rate, such as BMP-2 release for bone regeneration. Our results provided a scientific understanding of the mechanical performance of drug-eluting hydrogels and insights into designing hydrogels that can control the DR for biomedical applications such as bone regeneration and drug-delivery system.

■ ASSOCIATED CONTENT

Supporting Information

The Supporting Information is available free of charge at https://pubs.acs.org/doi/10.1021/acsomega.1c00824.

SEM image and size distribution of the HAPs; FTIR spectra of the HAP; XRD analysis of HAPs; DTG curves of the HAP/Col hydrogels; oscillation stress sweep of the HAP/Col hydrogels; BMP-2 release test; F−D curves of the HAP/Col hydrogels; and Young's modulus of the HAP/Col hydrogel (PDF)

■ AUTHOR INFORMATION

Corresponding Authors

Gyudo Lee − *Department of Biotechnology and Bioinformatics, Korea University, Sejong 30019, South Korea; Interdisciplinary Graduate Program for Artificial Intelligence Smart Convergence Technology, Korea University, Sejong 30019, South Korea;* orcid.org/0000-0001-7895-5112; Email: lkd0807@korea.ac.kr

Dae Sung Yoon − *School of Biomedical Engineering, Korea University, Seoul 02841, South Korea; Interdisciplinary Program in Precision Public Health, Korea University, Seoul 02841, South Korea*; Email: dsyoon@korea.ac.kr

Authors

Hyo Gi Jung − *School of Biomedical Engineering, Korea University, Seoul 02841, South Korea; Interdisciplinary Program in Precision Public Health, Korea University, Seoul 02841, South Korea;* orcid.org/0000-0001-5074-927X

Dongtak Lee − *School of Biomedical Engineering, Korea University, Seoul 02841, South Korea;* orcid.org/0000-0001-8716-1736

Sang Won Lee − *School of Biomedical Engineering, Korea University, Seoul 02841, South Korea*

Insu Kim − *School of Biomedical Engineering, Korea University, Seoul 02841, South Korea*

Yonghwan Kim − *School of Biomedical Engineering, Korea University, Seoul 02841, South Korea; Interdisciplinary Program in Precision Public Health, Korea University, Seoul 02841, South Korea*

Jae Won Jang − *School of Biomedical Engineering, Korea University, Seoul 02841, South Korea; Interdisciplinary Program in Precision Public Health, Korea University, Seoul 02841, South Korea*

Jeong Hoon Lee − *Department of Electrical Engineering, Kwangwoon University, Seoul 01897, South Korea*

Complete contact information is available at: https://pubs.acs.org/10.1021/acsomega.1c00824

Author Contributions

#H.G.J. and D.L. contributed equally to this work.

Notes

The authors declare no competing financial interest.

■ ACKNOWLEDGMENTS

This work was supported by the National Research Foundation of Korea (NRF) Grant funded by the Korean Government (MSIP) (No., NRF-2018M3C1B7020722, NRF-2019R1A2B5B01070617, NRF-2020R1A6A3A01096477, and NRF-2020R1A2C2102262). This study was also supported by the BK21 FOUR (Fostering Outstanding Universities for Research).

■ REFERENCES

(1) Caló, E.; Khutoryanskiy, V. V. Biomedical applications of hydrogels: A review of patents and commercial products. *Eur. Polym. J.* **2015**, *65*, 252−267.

(2) Zheng, J.; Fan, R.; Wu, H.; Yao, H.; Yan, Y.; Liu, J.; Ran, L.; Sun, Z.; Yi, L.; Dang, L. Directed self-assembly of herbal small molecules into sustained release hydrogels for treating neural inflammation. *Nat. Commun.* **2019**, *10*, 1−12.

(3) Devaraj, H.; Aw, K. C.; McDaid, A. J. Review of functional materials for potential use as wearable infection sensors in limb prostheses. *Biomed. Eng. Lett.* **2020**, *10*, 43−61.

(4) Hoare, T. R.; Kohane, D. S. Hydrogels in drug delivery: Progress and challenges. *Polymer* **2008**, *49*, 1993−2007.

(5) Ghasemiyeh, P.; Mohammadi-Samani, S. Hydrogels as Drug Delivery Systems; Pros and Cons. *J. Glob. Trends Pharm. Sci.* **2019**, *5*, 7−24.

(6) Li, J.; Mooney, D. J. Designing hydrogels for controlled drug delivery. *Nat. Rev. Mater.* **2016**, *1*, 1−17.

(7) Ehterami, A.; Salehi, M.; Farzamfar, S.; Samadian, H.; Vaez, A.; Sahrapeyma, H.; Ghorbani, S. A promising wound dressing based on

alginate hydrogels containing vitamin D3 cross-linked by calcium carbonate/d-glucono-δ-lactone. *Biomed. Eng. Lett.* **2020**, *10*, 309−319.
(8) Catoira, M. C.; Fusaro, L.; Di Francesco, D.; Ramella, M.; Boccafoschi, F. Overview of natural hydrogels for regenerative medicine applications. *J. Mater. Sci.: Mater.* **2019**, *30*, 115.
(9) Chung, Y.-I.; Ahn, K.-M.; Jeon, S.-H.; Lee, S.-Y.; Lee, J.-H.; Tae, G. Enhanced bone regeneration with BMP-2 loaded functional nanoparticle−hydrogel complex. *J. Controlled Release* **2007**, *121*, 91−99.
(10) Olthof, M. G.; Kempen, D. H.; Liu, X.; Dadsetan, M.; Tryfonidou, M. A.; Yaszemski, M. J.; Dhert, W. J.; Lu, L. Bone morphogenetic protein-2 release profile modulates bone formation in phosphorylated hydrogel. *J. Tissue. Eng. Regen. Med* **2018**, *12*, 1339−1351.
(11) Park, Y.; Sugimoto, M.; Watrin, A.; Chiquet, M.; Hunziker, E. B. BMP-2 induces the expression of chondrocyte-specific genes in bovine synovium-derived progenitor cells cultured in three-dimensional alginate hydrogel. *Osteoarthr. Cartil.* **2005**, *13*, 527−536.
(12) Park, K.-H.; Kim, H.; Moon, S.; Na, K. Bone morphogenic protein-2 (BMP-2) loaded nanoparticles mixed with human mesenchymal stem cell in fibrin hydrogel for bone tissue engineering. *J. Biosci. Bioeng.* **2009**, *108*, 530−537.
(13) Seo, B.-B.; Choi, H.; Koh, J.-T.; Song, S.-C. Sustained BMP-2 delivery and injectable bone regeneration using thermosensitive polymeric nanoparticle hydrogel bearing dual interactions with BMP-2. *J. Controlled Release* **2015**, *209*, 67−76.
(14) Kisiel, M.; Martino, M. M.; Ventura, M.; Hubbell, J. A.; Hilborn, J.; Ossipov, D. A. Improving the osteogenic potential of BMP-2 with hyaluronic acid hydrogel modified with integrin-specific fibronectin fragment. *Biomaterials* **2013**, *34*, 704−712.
(15) Lee, D.; Wufuer, M.; Kim, I.; Choi, T. H.; Kim, B. J.; Jung, H. G.; Jeon, B.; Lee, G.; Jeon, O. H.; Chang, H. Sequential dual-drug delivery of BMP-2 and alendronate from hydroxyapatite-collagen scaffolds for enhanced bone regeneration. *Sci. Rep.* **2021**, *11*, 1−10.
(16) George, J.; Hsu, C.-C.; Nguyen, L. T. B.; Ye, H.; Cui, Z. Neural tissue engineering with structured hydrogels in CNS models and therapies. *Biotechnol. Adv.* **2020**, *42*, 107370.
(17) Wong, R. S. H.; Dodou, K. Effect of drug loading method and drug physicochemical properties on the material and drug release properties of poly (ethylene oxide) hydrogels for transdermal delivery. *Polymer* **2017**, *9*, 286.
(18) Choi, J. R.; Yong, K. W.; Choi, J. Y.; Cowie, A. C. Recent advances in photo-crosslinkable hydrogels for biomedical applications. *BioTechniques* **2019**, *66*, 40−53.
(19) Mahdavinia, G. R.; Etemadi, H. In situ synthesis of magnetic CaraPVA IPN nanocomposite hydrogels and controlled drug release. *Mater. Sci. Eng. C* **2014**, *45*, 250−260.
(20) Ghanaatian, E.; Entezam, M. Mechanical properties and drug release rate of poly (vinyl alcohol)/poly (ethylene glycol)/clay nanocomposite hydrogels: Correlation with structure and physical properties. *J. Appl. Polym. Sci.* **2019**, *136*, 47843.
(21) Martinez, A. W.; Caves, J. M.; Ravi, S.; Li, W.; Chaikof, E. L. Effects of crosslinking on the mechanical properties, drug release and cytocompatibility of protein polymers. *Acta Biomater.* **2014**, *10*, 26−33.
(22) Vedadghavami, A.; Minooei, F.; Mohammadi, M. H.; Khetani, S.; Kolahchi, A. R.; Mashayekhan, S.; Sanati-Nezhad, A. Manufacturing of hydrogel biomaterials with controlled mechanical properties for tissue engineering applications. *Acta Biomater.* **2017**, *62*, 42−63.
(23) Walker, J. M.; Myers, A. M.; Schluchter, M. D.; Goldberg, V. M.; Caplan, A. I.; Berilla, J. A.; Mansour, J. M.; Welter, J. F. Nondestructive evaluation of hydrogel mechanical properties using ultrasound. *Ann. Biomed. Eng.* **2011**, *39*, 2521.
(24) Oyen, M. Mechanical characterisation of hydrogel materials. *Int. Mater. Rev.* **2014**, *59*, 44−59.
(25) Lee, H.; Hong, Y.; Lee, D.; Hwang, S.; Lee, G.; Yang, J.; Yoon, D. S. Surface potential microscopy of surfactant-controlled single gold nanoparticle. *Nanotechnology* **2020**, *31*, 215706.
(26) Lee, H.; Lee, S. W.; Lee, G.; Lee, W.; Lee, J. H.; Hwang, K. S.; Yang, J.; Lee, S. W.; Yoon, D. S. Kelvin probe force microscopy of DNA-capped nanoparticles for single-nucleotide polymorphism detection. *Nanoscale* **2016**, *8*, 13537−13544.
(27) Dufrêne, Y. F.; Ando, T.; Garcia, R.; Alsteens, D.; Martinez-Martin, D.; Engel, A.; Gerber, C.; Müller, D. J. Imaging modes of atomic force microscopy for application in molecular and cell biology. *Nat. Nanotechnol.* **2017**, *12*, 295−307.
(28) Carl, P.; Schillers, H. Elasticity measurement of living cells with an atomic force microscope: data acquisition and processing. *Pflügers Arch.* **2008**, *457*, 551.
(29) Offroy, M.; Razafitianamaharavo, A.; Beaussart, A.; Pagnout, C.; Duval, J. F. Fast automated processing of AFM PeakForce curves to evaluate spatially resolved Young modulus and stiffness of turgescent cells. *RSC Adv.* **2020**, *10*, 19258−19275.
(30) Te Riet, J.; Katan, A. J.; Rankl, C.; Stahl, S. W.; van Buul, A. M.; Phang, I. Y.; Gomez-Casado, A.; Schön, P.; Gerritsen, J. W.; Cambi, A. Interlaboratory round robin on cantilever calibration for AFM force spectroscopy. *Ultramicroscopy* **2011**, *111*, 1659−1669.
(31) Dimitriadis, E. K.; Horkay, F.; Maresca, J.; Kachar, B.; Chadwick, R. S. Determination of elastic moduli of thin layers of soft material using the atomic force microscope. *Biophys. J.* **2002**, *82*, 2798−2810.
(32) Doyle, A. D. Generation of 3D collagen gels with controlled diverse architectures. *Curr. Protoc. Cell. Biol* **2016**, *72*, 9.
(33) Terajima, M.; Perdivara, I.; Sricholpech, M.; Deguchi, Y.; Pleshko, N.; Tomer, K. B.; Yamauchi, M. Glycosylation and cross-linking in bone type I collagen. *J. Biol. Chem.* **2014**, *289*, 22636−22647.
(34) Termine, J. D.; Kleinman, H. K.; Whitson, S. W.; Conn, K. M.; McGarvey, M. L.; Martin, G. R. Osteonectin, a bone-specific protein linking mineral to collagen. *Cell* **1981**, *26*, 99−105.
(35) Ku, M.; Kim, H. J.; Yau, S. Y.; Yoon, N.; Kim, N. H.; Yook, J. I.; Suh, J. S.; Kim, D. E.; Yang, J. Microsphere-Based Nanoindentation for the Monitoring of Cellular Cortical Stiffness Regulated by MT1-MMP. *Small* **2018**, *14*, No. 1803000.
(36) Ficai, A.; Andronescu, E.; Voicu, G.; Ghitulica, C.; Vasile, B. S.; Ficai, D.; Trandafir, V. Self-assembled collagen/hydroxyapatite composite materials. *Chem. Eng. J.* **2010**, *160*, 794−800.
(37) Riaz, T.; Zeeshan, R.; Zarif, F.; Ilyas, K.; Muhammad, N.; Safi, S. Z.; Rahim, A.; Rizvi, S. A.; Rehman, I. U. FTIR analysis of natural and synthetic collagen. *Appl. Spectrosc. Rev.* **2018**, *53*, 703−746.
(38) Teng, S. H.; Lee, E. J.; Wang, P.; Shin, D. S.; Kim, H. E. Three-layered membranes of collagen/hydroxyapatite and chitosan for guided bone regeneration. *J. Biomed. Mater. Res.* **2008**, *87B*, 132−138.
(39) Anbalagan Balamurugan, J. M.; Faure, J.; HichamBenhayoune, L.; Sockallingum, G.; Banchet, V.; Bouthors, S.; Laurent-Maquin, D.; Balossier, G. Synthesis and structural analysis of sol-gel derived stoichiometric monophasic hydroxyapatite. *Ceram. - Silik.* **2006**, *50*, 27−31.
(40) Zhang, L.-J.; Feng, X.-S.; Liu, H.-G.; Qian, D.-J.; Zhang, L.; Yu, X.-L.; Cui, F.-Z. Hydroxyapatite/collagen composite materials formation in simulated body fluid environment. *Mater. Lett.* **2004**, *58*, 719−722.
(41) Lawyer, T.; McIntosh, K.; Clavijo, C.; Potekhina, L.; Mann, B. K. Formulation changes affect material properties and cell behavior in HA-based hydrogels. *Int. J. Cell Biol.* **2012**, *2012*, 1.
(42) Roveri, N.; Falini, G.; Sidoti, M.; Tampieri, A.; Landi, E.; Sandri, M.; Parma, B. Biologically inspired growth of hydroxyapatite nanocrystals inside self-assembled collagen fibers. *Mater. Sci. Eng. C* **2003**, *23*, 441−446.
(43) Sionkowska, A.; Kozłowska, J. Characterization of collagen/hydroxyapatite composite sponges as a potential bone substitute. *Int. J. Biol. Macromol.* **2010**, *47*, 483−487.
(44) Song, W.; Markel, D. C.; Jin, X.; Shi, T.; Ren, W. Poly (vinyl alcohol)/collagen/hydroxyapatite hydrogel: Properties and in vitro cellular response. *J. Biomed. Mater. Res. Part A* **2012**, *100A*, 3071−3079.

https://doi.org/10.1021/acsomega.1c00824
ACS Omega 2021, 6, 9269−9278

(45) Pelin, I. M.; Maier, S. S.; Chitanu, G. C.; Bulacovschi, V. Preparation and characterization of a hydroxyapatite−collagen composite as component for injectable bone substitute. *Mater. Sci. Eng. C* **2009**, *29*, 2188−2194.
(46) Cuomo, F.; Cofelice, M.; Lopez, F. Rheological characterization of hydrogels from alginate-based nanodispersion. *Polymer* **2019**, *11*, 259.
(47) Dhivya, S.; Saravanan, S.; Sastry, T.; Selvamurugan, N. Nanohydroxyapatite-reinforced chitosan composite hydrogel for bone tissue repair in vitro and in vivo. *J. Nanobiotechnology* **2015**, *13*, 40.
(48) Boix, T.; Gomez-Morales, J.; Torrent-Burgues, J.; Monfort, A.; Puigdoménech, P.; Rodriguez-Clemente, R. Adsorption of recombinant human bone morphogenetic protein rhBMP-2m onto hydroxyapatite. *J. Inorg. Biochem.* **2005**, *99*, 1043−1050.
(49) Ma, X.; He, Z.; Han, F.; Zhong, Z.; Chen, L.; Li, B. Preparation of collagen/hydroxyapatite/alendronate hybrid hydrogels as potential scaffolds for bone regeneration. *Colloids Surf., B* **2016**, *143*, 81−87.
(50) Morin, R.; Kaplan, D.; Perez-Ramirez, B. Bone morphogenetic protein-2 binds as multilayers to a collagen delivery matrix: an equilibrium thermodynamic analysis. *Biomacromolecules* **2006**, *7*, 131−138.
(51) Meyvis, T.; De Smedt, S.; Demeester, J.; Hennink, W. Influence of the degradation mechanism of hydrogels on their elastic and swelling properties during degradation. *Macromolecules* **2000**, *33*, 4717−4725.
(52) Suvarnapathaki, S.; Wu, X.; Lantigua, D.; Nguyen, M. A.; Camci-Unal, G. Hydroxyapatite-Incorporated Composite Gels Improve Mechanical Properties and Bioactivity of Bone Scaffolds. *Macromol. Biosci.* **2020**, *20*, No. 2000176.
(53) Pistone, A.; Iannazzo, D.; Celesti, C.; Scolaro, C.; Giofré, S. V.; Romeo, R.; Visco, A. Chitosan/PAMAM/Hydroxyapatite Engineered Drug Release Hydrogels with Tunable Rheological Properties. *Polymer* **2020**, *12*, 754.
(54) Selby, A.; Maldonado-Codina, C.; Derby, B. Influence of specimen thickness on the nanoindentation of hydrogels: measuring the mechanical properties of soft contact lenses. *J. Mech. Behav. Biomed. Mater.* **2014**, *35*, 144−156.
(55) Zhu, Y.; Dong, Z.; Wejinya, U. C.; Jin, S.; Ye, K. Determination of mechanical properties of soft tissue scaffolds by atomic force microscopy nanoindentation. *J. Biomech.* **2011**, *44*, 2356−2361.

https://doi.org/10.1021/acsomega.1c00824
ACS Omega 2021, 6, 9269−9278